An essential role for functional lysosomes in ferroptosis of cancer cells

Seiji Torii*[1,2], Ryosuke Shintoku*†[1], Chisato Kubota*[1], Makoto Yaegashi*, Ryoko Torii*, Masaya Sasaki‡, Toshinobu Suzuki‡, Masanobu Mori‡, Yuhei Yoshimoto†, Toshiyuki Takeuchi* and Keiichi Yamada§

*Secretion Biology Laboratory, Institute for Molecular and Cellular Regulation, Gunma University, Maebashi 371-8512, Japan
†Department of Neurosurgery, Gunma University Graduate School of Medicine, Maebashi 371-8512, Japan
‡Department of Environmental Engineering Science, Graduate School of Science and Technology, Gunma University, Kiryu 376-8515, Japan
§Department of Chemistry and Chemical Biology, Graduate School of Science and Technology, Gunma University, Kiryu 376-8515, Japan

Pharmacological challenges to oncogenic Ras-expressing cancer cells have shown a novel type of cell death, ferroptosis, which requires intracellular iron. In the present study, we assessed ferroptosis following treatment of human fibrosarcoma HT1080 cells with several inhibitors of lysosomal activity and found that they prevented cell death induced by the ferroptosis-inducing compounds erastin and RSL3. Fluorescent analyses with a reactive oxygen species (ROS) sensor revealed constitutive generation of ROS in lysosomes, and treatment with lysosome inhibitors decreased both lysosomal ROS and a ferroptotic cell-death-associated ROS burst. These inhibitors partially prevented intracellular iron provision by attenuating intracellular transport of transferrin or autophagic degradation of ferritin. Furthermore, analyses with a fluorescent sensor that detects oxidative changes in cell membranes revealed that formation of lipid ROS in perinuclear compartments probably represented an early event in ferroptosis. These results suggest that lysosomal activity is involved in lipid ROS-mediated ferroptotic cell death through regulation of cellular iron equilibria and ROS generation.

Key words: autophagy, iron, necrosis, oxidative stress, Ras.

INTRODUCTION

Cell death plays an important role in the normal development and homoeostasis of living individuals, and is also implicated in abnormal activities of these processes in several diseases. Cells possess multiple cell death programmes including apoptosis and necrosis, which are mutually connected and can occur in response to defects in different pathways [1]. Studies involving genetics and chemical biology have revealed the existence of several regulated types of necrosis [2,3], with iron-related cell death, or ferroptosis, being proposed by Stockwell and colleagues [3]. Ferroptosis is induced in oncogenic Ras-expressing cells by a number of small compounds referred to as ferroptosis inducers (FINs), which include erastin and RSL3 [3–6]. Ferroptosis can be characterized at a morphological level by the presence of shrunken mitochondria, and is functionally independent of caspases, ATP depletion or mitochondrial outer membrane permeabilization. Ferroptosis requires intracellular iron that may induce reactive oxygen species (ROS) production and lipid peroxidation [3–7].

The ferroptotic cell death pathway has been classified into two types where: (i) glutathione (GSH) depletion results from inhibition of system x_c^- by class-I FINs (e.g. erastin), and (ii) glutathione peroxidase 4 (GPx4) activity is directly inhibited by class-II FINs (e.g. RSL3) [6]. Erastin has three main target proteins: the cell-surface cystine/glutamate antiporter (system x_c^-: SLC7A11/SLC3A2 complex), the large neutral amino acid transporter (system L: SLC7A5/SLC3A2 complex), and mitochondrial voltage-dependent anion channels [4,5]. However, ferroptotic cell death requires a remarkable reduction in GSH that is triggered by direct impairment of cystine uptake by system x_c^- [6]. GSH depletion in turn inhibits GSH-dependent peroxidases (GPxs), particularly GPx4, which is a unique enzyme that reduces lipid hydroperoxides in cell membranes [8]. Pronounced accumulation of lipid ROS via GPx4 suppression is thought to be critical for the execution of ferroptotic cell death, because compounds related to the membrane antioxidant vitamin E (e.g. 6-hydroxy-2,5,7,8-tetramethylchroman-2-carboxylic acid: Trolox) have been shown to prevent both FIN-induced and GPx4 knockdown-induced cell death [6,7]. Moreover, (1*S*,3*R*)-RSL3, a typical class-II FIN, interacts with GPx4 directly and prevents its activity, whereas GPx4 overexpression and inhibition suppresses and enhances FIN-induced ferroptosis, respectively, which indicates that GPx4 is a central regulator of ferroptotic cell death [6].

GPx4 is thought to be the limiting GSH-dependent enzyme, because GPx4-knockout mice die at 7.5 days, which is the same day on which mice lacking GSH-synthesizing enzymes die [9–11]. Inducible genetic deletion of GPx4 in mouse embryonic fibroblasts leads to cell death in response to 12/15-lipoxygenase (12/15-LOX)-dependent lipid peroxidation [12]. Similar signalling pathways have been suggested to be important for neuronal oxidative toxicity caused by acute cerebral ischaemia. In cell model systems, excess glutamate triggers cell death of neurons by a decrease in GSH and an associated activation of 12/15-LOX [13]. Furthermore, glutamate-induced cell death in brain slices can be prevented by the ferroptosis inhibitor ferrostatin 1 (Fer-1) that serves as an antioxidant in membranes, suggesting that neuronal cell death and ferroptosis share several common molecules and pathways [3]. More recently, acute renal injury in mice was shown to involve cell death that has several

Abbreviations: Baf A_1, bafilomycin A_1; BFP, blue fluorescent protein; CM-H_2DCFDA, 5-(and-6-)chloromethyl-2′,7′-dichlorodihydrofluorescein diacetate; DFO, deferoxamine; DMEM, Dulbecco's modified Eagle's medium; FAAS, flame atomic absorbance spectrophotometer; Fer-1, ferrostatin 1; FIN, ferroptosis inducer; GPx4, glutathione peroxidase 4; ICT1, immature colon carcinoma cell transcript 1; LDH, lactate hydrogenase; 12/15-LOX, 12/15-lipoxygenase; 3-MA, 3-methyladenine; M6PR, mannose 6-phosphate receptor; NOX, NADPH oxidase; PepA-Me, pepstatin A-methyl ester; PF-H_2TMRos, 2,3,4,5,6-pentafluorodihydrotetramethylrosamine; ROS, reactive oxygen species; RP, reverse-phase; TFR1, transferrin receptor 1.

[1] These authors contributed equally to this work.

[2] To whom correspondence should be addressed (email storii@gunma-u.ac.jp).

characteristics of ferroptosis, including lipid peroxidation, and treatment with Fer-1 or its related agents can prevent this type of cell death [14,15]. These observations indicate that ferroptosis occurs not only in cells or tissues but also *in vivo*.

The susceptibility of cancer cells to ferroptosis appears to be related to constitutive activation of Ras-MEK signalling [3–5], which can contribute to iron abundance in tumours by altering the expression levels of the transferrin receptor and ferritin [4]. Generally, iron enters cells by internalization of transferrin receptors bound to transferrin–$Fe(III)_2$ [16]. The ferric ion that is released from transferrin is reduced by an endosomal reductase activity (e.g. six-transmembrane epithelial antigen of the prostate 3) prior to export of ferrous ion by a transporter such as divalent metal transporter 1 (DMT1). Most cellular iron is stored as a component of ferritin in the Fe(III) form. The labile iron pool is presumably used to control intracellular iron homoeostasis through its own redox activity or to provide iron constituents for functional proteins such as haem enzymes. Several ROS-generating enzymes, including LOX and NADPH oxidases (NOXs) require iron or its derivatives for their activity. Interestingly, the pentose phosphate and NOX pathway may contribute to erastin-induced ferroptotic cell death [3], whereas oncogenic Ras reportedly induces rapid production of ROS partly by up-regulating levels of NOX1 [17,18]. In contrast, redox-active iron catalyses Fenton-type reactions for the direct production of ROS, such as the hydroxyl radical, which is thought to oxidize cell constituents that in turn cause damage to cell structures and integrity. *In vitro*, the initiation of lipid peroxidation requires both ferric and ferrous ions, and the ratio of Fe(III) to Fe(II) is important in determining its rate [19]. However, how iron contributes to ferroptosis in conjunction with ROS is unclear.

In the present study, we used N-Ras-mutant HT1080 cells to examine how specific organelles and spatial dynamics of ROS contribute to ferroptosis. We evaluated various chemical reagents for their ability to protect tumour cells from death, and found that lysosome inhibitors repressed cell death by reducing basal ROS generation in these compartments. Our data suggest that endosomes/lysosomes are essential for the iron metabolism in ferroptosis-sensitive cells.

EXPERIMENTAL

Inhibitors

Erastin and the aspartic protease inhibitor pepstatin A-methyl ester (PepA-Me) were purchased from Calbiochem. Bafilomycin A_1 (Baf A_1), an inhibitor of vacuolar H^+-ATPase, was purchased from Wako. The iron chelator deferoxamine (DFO) was purchased from Sigma.

Synthesis of RSL3

RSL3 was synthesized from L-tryptophan methyl ester hydrochloride (HCl·H-Trp-OMe, Kokusan Chemical) according to a previously described method [20]. The corresponding RSL3 intermediate (mixture) was dissolved in chloroform and potassium carbonate (1.1 equiv.) was added. Chloroacetyl chloride (1.0 equiv.) was then added dropwise to the stirred solution at 0 °C. The reaction mixture was stirred overnight at room temperature and filtered. The filtrate was extracted by water and the organic layer washed with brine before drying over anhydrous sodium sulfate. After filtering the sodium sulfate, the filtrate was concentrated *in vacuo* to yeild the crude product, which was revealed by reverse-phase (RP)-HPLC analysis to contain mainly two products (Supplementary Figure S1a). These two compounds were both identified as RSL3 by ESI–MS that were acquired with an Applied Biosystems API-2000 mass spectrometer (positive ion mode). The former product identified by RP-HPLC (Supplementary Figure S1b) was used for the following experiment with MS (ESI, *m*/*z*): $[M\text{-H}]+$ $C_{23}H_{21}ClN_2O_5$, calculated, 440.1; actual 440.9.

Cell culture and ferroptosis induction

HT1080 (human fibrosarcoma) and Calu-1 (human non-small-cell lung cancer) cells were cultured in Dulbecco's modified Eagle's medium (DMEM) and Eagle's minimum essential medium with Earle's salts, respectively, which both contained 10 % FBS. For ferroptosis induction, cells were plated at 1.0×10^5 cells per well on six-well plates and cultured for 36 h. Culture medium was replaced with 1 ml of medium containing 5 or 10 μM erastin or 1 μM RSL3 with or without inhibitors. Cell viability was determined by Trypan Blue dye-exclusion assay. HT1080 or Calu-1 cells were collected at the indicated time and incubated with 0.4 % Trypan Blue, and observed under a microscope where stained and unstained cells were counted separately with a haemocytometer. Because cells that had undergone ferroptosis were sometimes lost during the assay procedure, the cell survival rate was calculated according to the following formula: cell survival (%) = unstained cells number (drug treated/untreated) × 100. For the lactate dehydrogenase (LDH) assay, medium was collected at the indicated time and each LDH activity was measured by a CytoTox 96 cytotoxicity assay (Promega).

Transfection

A vector expressing EGFP-tagged Atg4B-C74A was constructed as described previously [21]. cDNAs of cation-dependent mannose 6-phosphate receptor (M6PR) [21] and immature colon carcinoma cell transcript 1 (ICT1) were subcloned into pTagBFP2 vector (Evrogen). The siRNA against human transferrin receptor 1 (TFR1) was designed and synthesized by Integrated DNA Technologies (code number HSC.RNAI.N001128148.12.3). Transfections were performed with HilyMax reagent (Dojindo Molecular Technologies), and 75 % transfection efficiency was observed with a reporter gene (results not shown).

Fluorescence detection of ROS

HT1080 cells were incubated on poly-L-lysine (Sigma)-coated coverslips in the dark at 37 °C with 5 μM BODIPY-(581/591)-C_{11} (Invitrogen) or with 5 μM 2,3,4,5,6-pentafluorodihydrotetramethylrosamine (PF-H_2TMRos) (Invitrogen) for 30 min. The cells were mounted on a glass slide with Hank's buffer. Dye oxidation, indicated by PF-TMRos red fluorescence and a shift in BODIPY fluorescence from red to green, was observed with a Keyence BZ-9000 microscope or with an epifluorescence microscope (Olympus BX-50) equipped with a SenSys™ charge-coupled device camera (Photometrics) as described previously [21]. Co-localization with organelle markers was observed with an LSM5 PASCAL confocal microscope (Carl Zeiss) or FV10i-DOC confocal microscope (Olympus). To avoid indicator dye photo-oxidation, fluorescence images were collected by a single rapid scan with identical parameters (e.g. contrast and brightness) for all samples. For BODIPY-C_{11}, fluorescence images detected with appropriate cut-off filters were simultaneously collected to compare oxidized (green) and

unoxidized dye (red). Fluorescence intensity was quantified using ImageJ 1.40g (NIH).

Western blot analysis

Immunoblotting was performed as described previously [22]. Blotted membranes were blocked with 5 % non-fat dried skimmed milk powder for 30 min, and incubated with primary antibodies (1:1000 dilution of rabbit anti-ferritin, Abcam, or 1:10000 dilution of mouse anti-biotin, Jackson ImmunoResearch).

Transferrin uptake assay

Prior to transferrin loading, cells were treated with each inhibitor (DFO, ammonium chloride, Baf A_1, PepA-Me) for 1 h and then loaded with biotin–transferrin (10 μg/ml; Invitrogen) or Alexa Fluor 488–transferrin (50 μg/ml; Invitrogen) for cumulative uptake at 37 °C for 30 and 20 min respectively. Cells containing biotin–transferrin were washed and extracted in lysis buffer (20 mM Tris/HCl, pH 7.5, 150 mM NaCl, 0.5 % Nonidet P-40, 1 mM EGTA, 0.5 mM PMSF, 10 μg/ml aprotinin, 10 μg/ml leupeptin and 10 μg/ml pepstatin). Cell extracts (5 μg) were then analysed by immunoblotting with anti-biotin antibody. Immunoreactive band intensity was measured by densitometry, quantified using ImageJ and normalized relative to the control sample (no inhibitors) in the same membrane.

Intracellular iron measurement

HT1080 cells seeded on two 100-mm-diameter dishes were incubated with or without inhibitors for 5 h. For evaluation of transferrin receptor, siRNA-transfected cells were pre-incubated in DMEM without serum for 30 min and then treated with 0.01 mg/ml human holo-transferrin (Sigma) for 8 h. Cells were washed with PBS and the collected cells were lysed in 80 % HNO_3/20 % H_2O_2 for 24 h at room temperature. The total iron content in each diluted sample was determined using a Z-5300 flame atomic absorbance spectrophotometer (FAAS: Hitachi).

Statistical analysis

Data are presented as means ± S.E.M. Non-parametric data were compared using the Kruskal–Wallis test, followed by the Steel test.

RESULTS

We first examined the effects of the ferroptosis-inducing reagents erastin and RSL3 on human fibrosarcoma HT1080 cells. To avoid the loss of dead cells, the number of live cells was determined by Trypan Blue dye-exclusion assays. Treatment with erastin (5 and 10 μM) had little effect on cell survival within 6 h, but by 8 h most of the cells had died (Supplementary Figure S2A). RSL3 was the more potent FIN reagent and even at a low dose (1 μM) induced rapid cell death in HT1080 cells (Supplementary Figure S2A) and another cancer cell line (results not shown). The potency of these reagents is consistent with their target proteins and the signal pathways that were demonstrated by the Stockwell group [3,6]. As previously reported, the free iron chelator DFO prevented erastin-induced cell death (Supplementary Figure S2B) even when it was added after erastin treatment. Baf A_1 (0.4 μM), which is a specific vacuolar ATPase inhibitor, also protected HT1080 cells from erastin toxicity (Supplementary Figure S2B and Figure 1A), although earlier studies had suggested that this inhibitor was ineffective [3]. In the present study, we found that Baf A_1 (>1 μM) alone induced some cell death (presumably apoptosis) when incubated with the cells for longer time periods (>16 h) (results not shown). In addition to Baf A_1, ammonium chloride (10 mM), which acts to neutralize acidic organelles such as the lysosome, and the lysosomal aspartic protease inhibitor PepA-Me (25 μM) also blocked erastin-induced cell death completely at 8 h (Figure 1A). Similarly, the viability of lung cancer Calu-1 cells began to decline at 10 h after erastin treatment, and all of the above-described inhibitors also prevented ferroptosis even at the 24 h time point (Figure 1B). Cell damage was further assessed by a LDH release assay. Baf A_1, ammonium chloride and PepA-Me all significantly protected cells from erastin- or RSL3-induced cell death (Figures 1C and 1D), suggesting that basal lysosomal activities are involved in ferroptotic cell death in these cells.

Next, the contribution of autophagy to ferroptosis was examined in the presence of 3-methyladenine (3-MA), which is generally used as a macroautophagy inhibitor. When the number of viable cells was calculated at the 8 h time point, a significant reduction in cell death was observed in the presence of 3-MA, although the inhibitory effect of this compound was lower than that seen for the lysosomal inhibitors (Figure 1E). We next used an inactive mutant of Atg4B protease (Atg4B-C74A), which sequesters the LC3 protein and blocks formation of the Atg7-LC3 intermediate [23]. Overexpression of EGFP-tagged Atg4B-C74A induced some levels of apoptosis in untreated cells (results not shown), suggesting that basal autophagic activity is required for HT1080 cell survival. Importantly, this mutant protease significantly reduced erastin-induced cell death compared with control cells (Figure 1F). These observations suggest that both autophagic activity and lysosomal function are involved in FIN-induced ferroptosis in Ras tumour cell lines.

Because erastin-induced ferroptosis is accompanied by an accumulation of ROS and an associated lipid peroxidation [3,6,7], we next used the fluorescent probe PF-H_2TMRos to examine whether ROS levels were increased in erastin-treated HT1080 cells. As with the widely available probe 5-(and-6-)chloromethyl-2′,7′-dichlorodihydrofluorescein diacetate (CM-H_2DCFDA), the general ROS sensor PF-H_2TMRos can detect cell-death-associated ROS bursts [21]. Microscopic applications using the PF-H_2TMRos probe are also useful in observing the intracellular localization of ROS, because this probe is less sensitive to photo-oxidation than is CM-H_2DCFDA. As shown in Figure 2A, erastin treatment evoked intense PF-TMRos red fluorescence, which became prominent at approximately 7 h. Consistent with earlier reports, the erastin-induced ROS burst was detected largely in the cytosol [3,6,7]. The finding that fluorescence intensity remained low in cells treated with Baf A_1, ammonium chloride or PepA-Me (Figure 2B) suggests the involvement of lysosomes in the ROS burst. We then assessed the effects of inhibitors on lipid ROS production using the membrane peroxidation sensor BODIPY-C_{11}, and confirmed that lipid ROS levels did not increase in these cells that had modified lysosome activity (Figure 2C). Similar observations were made in cells treated with the autophagy inhibitors 3-MA and chloroquine (results not shown). Therefore, inhibitors of autophagy and lysosomal activity both reduced erastin-induced ferroptosis, which is probably due to the activity of the agents in preventing cytosolic and lipid ROS production.

Because acidic organelles such as endosomes and lysosomes are required for iron uptake and release, we examined whether these lysosome-related inhibitors could alter iron equilibria. The total cellular iron concentration was first determined using a FAAS. FAAS analyses revealed that PepA-Me treatment

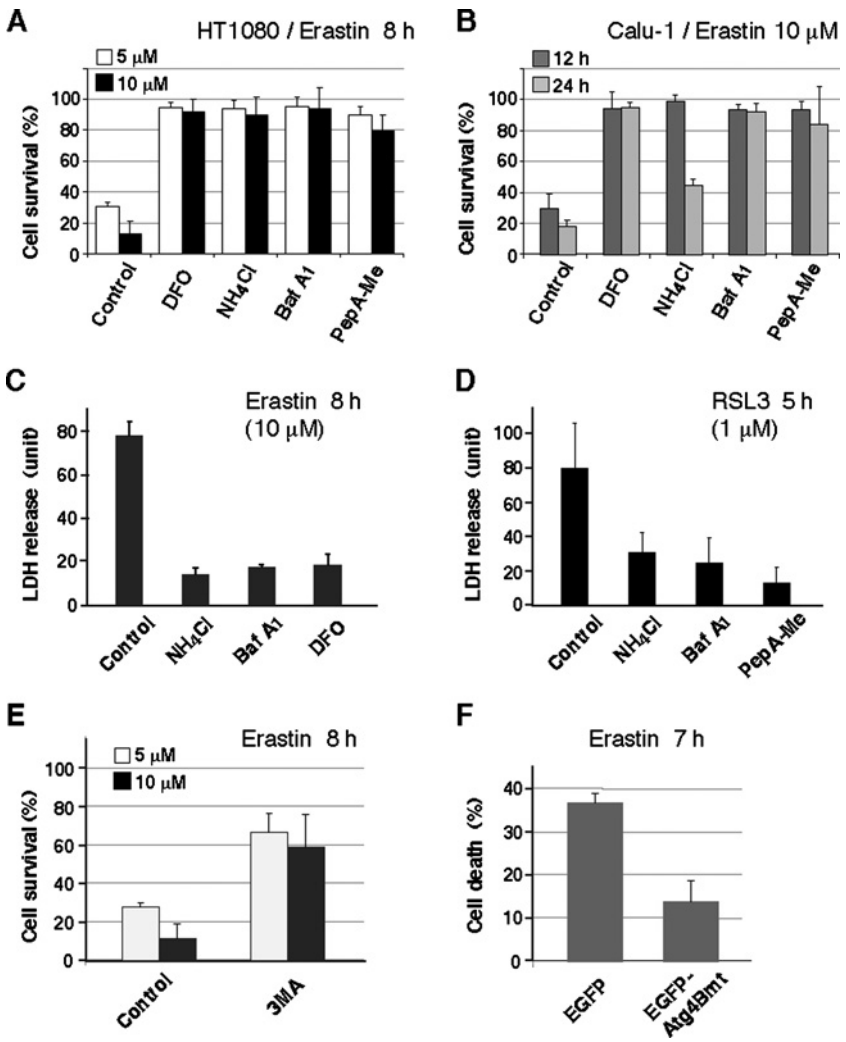

Figure 1 Lysosome/autophagy inhibitors suppress FIN-induced ferroptosis

(**A**) HT1080 cells were treated with 5 or 10 μM erastin in the presence or absence of each inhibitor for 8 h. Cell viability was determined by Trypan Blue dye-exclusion assay. Cell survival rates are presented as the mean $\pm$ S.E.M. ($n = 4$) percentages of live cells relative to control cell numbers (DMSO-treated cells) using DFO (0.1 mM), Baf A_1 (0.4 μM), ammonium chloride (10 mM) or PepA-Me (25 μM). (**B**) Calu-1 cells were treated with 10 μM erastin in the presence or absence of each inhibitor for 12 or 24 h. Cell viability was determined, and the values were calculated as described for (**A**). (**C**) HT1080 cells were treated as in (**A**) and cell death rates were then determined by a secreted LDH activity assay. Results are the means $\pm$ S.E.M. for three independent experiments. (**D**) HT1080 cells were treated with 1 μM RSL3 in the presence or absence of each inhibitor for 5 h. The cell death rate was determined by LDH assay. Results are the means $\pm$ S.E.M. for three independent experiments. (**E**) HT1080 cells were treated with 5 or 10 μM erastin for 8 h with or without 3-MA. The cell survival rate is presented as the mean $\pm$ S.E.M. ($n = 3$) percentages of live treated cells relative to control cell numbers (DMSO). (**F**) Cells transfected with EGFP-Atg4B-C74A or EGFP were treated with 5 μM erastin. After incubation for 7 h, the cell death rate was determined by Trypan Blue dye-exclusion assay. Results are the means $\pm$ S.E.M. for three independent experiments. $P < 0.05$; Kruskal–Wallis test followed by Steel test.

caused a significant decrease in the cellular iron content that was comparable to the effect produced by DFO treatment (Figure 3A). Meanwhile, other reagents (Baf A_1 and ammonium chloride) did not induce any significant decrease in iron levels. Cytosolic ferritin is known to be degraded within lysosomes via a specific autophagic pathway [24,25] that releases free iron for use. Thus, ferritin protein levels were analysed by immunoblotting with an anti-ferritin antibody. An obvious up-regulation of ferritin protein was detected in PepA-Me-treated cells (Figure 3B), suggesting that PepA-Me induces the iron content reduction by inhibiting ferritin degradation in lysosomes. Transferrin uptake was next examined by incubating cells with Alexa Fluor 488-conjugated transferrin. In control cells the endocytosed fluorescent transferrin was distributed sparsely around the perinuclear region, whereas Baf A_1 and PepA-Me-treated cells displayed reduced punctate signals and puncta that were concentrated in regions with microtubule-organizing centres (Figure 3C). Meanwhile, transferrin fluorescence signals apparently declined in cells treated with ammonium chloride, although the overall distribution pattern did not change. The rate of transferrin uptake was then quantified by measuring the extent of biotin-labelled transferrin using immunoblotting. Ammonium chloride-treated cells consistently exhibited a lower rate of biotin–transferrin uptake relative to untreated cells (Figure 3C, histogram), suggesting that acidic organelles are important for iron homoeostasis. We then employed siRNA to suppress TFR1 expression. Silencing of TFR1 efficiently suppressed fluorescent transferrin uptake and also reduced iron uptake from transferrin (Figure 3D), whereas some TFR1-independent iron-uptake pathways were suggested [26]. TFR1 knockdown led to a marked decrease in the cell death rate in cells incubated with erastin (Figure 3D, histogram), suggesting that transferrin-mediated iron uptake is essential for ferroptotic cell death.

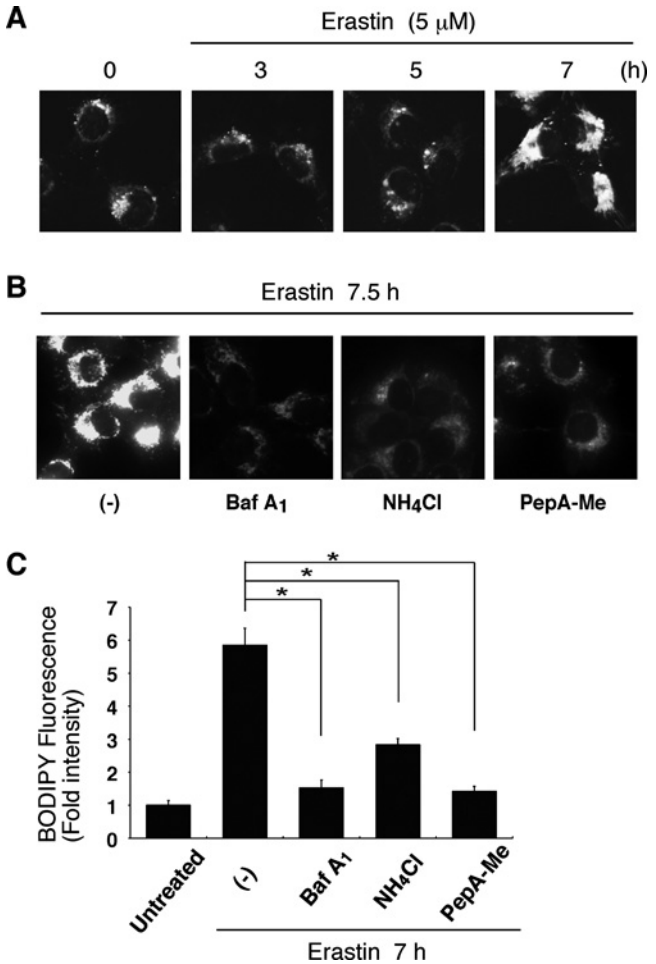

Figure 2 ROS generation is blocked by lysosome inhibitors

(**A**) HT1080 cells were treated with 5 μM erastin for the indicated times. The cells were then incubated with 5 μM PF-H_2TMRos for 30 min, and PF-TMRos fluorescence signals were visualized by microscopy with constant fluorescence parameters. (**B**) Cells were treated with 5 μM erastin in the presence or absence of each inhibitor for 7.5 h and then incubated with PF-H_2TMRos. Resulting fluorescence signals were visualized by microscopy with constant fluorescence parameters. (**C**) HT1080 cells were treated with 5 μM erastin in the presence or absence of each inhibitor for 7 h. The cells were then incubated with 5 μM BODIPY-(581/591)-C_{11} for 30 min. Green and red fluorescence signals were separately visualized by microscopy with constant fluorescence parameters. The intensity of green fluorescence in each cell was quantified with a densitometric imager, and the results from three independent experiments are presented as mean fold-increases $\pm$ S.E.M. relative to that of the control (untreated). *$P < 0.05$.

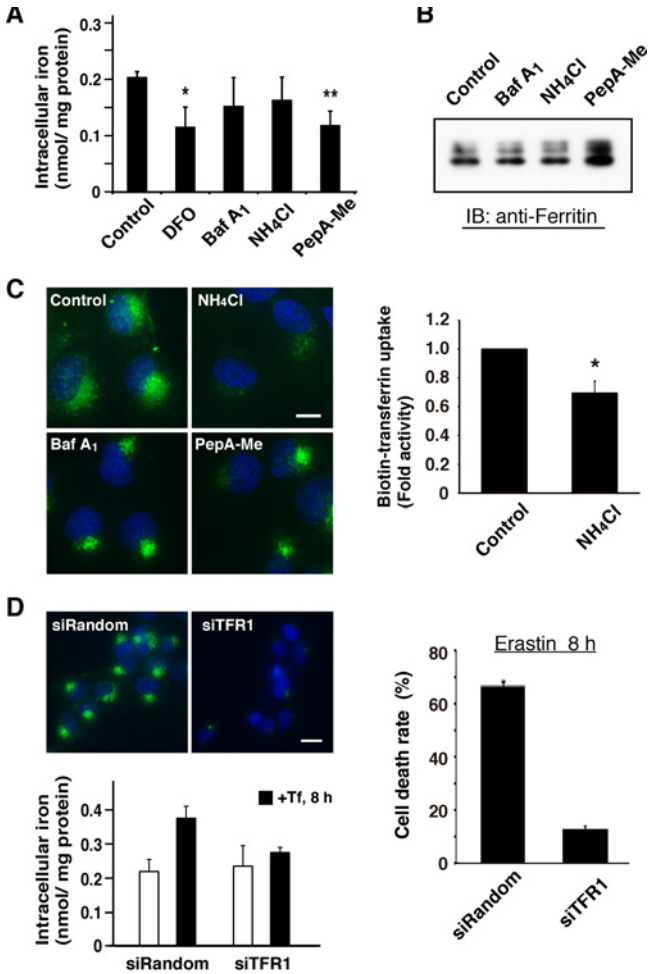

Figure 3 Effects of lysosome inhibitors on intracellular iron transport and storage

(**A**) HT1080 cells were incubated with each inhibitor for 5 h before they were dissolved in nitric acid. The iron concentration was measured with a FAAS. Cumulative data are presented as the means $\pm$ S.E.M. for five independent experiments. *$P < 0.05$, **$P < 0.01$. (**B**) Cells were incubated with each inhibitor for 12 h, and then lysed. Each cell lysate was subjected to immunoblot analysis with anti-ferritin antibody. Experiments were repeated three times with reproducible results. (**C**) Left panel: HT1080 cells were treated with each inhibitor for 1 h and then incubated with 50 μg/ml Alexa Fluor 488–transferrin for 20 min. The cells were fixed and green fluorescence signals were visualized by microscopy with constant fluorescence parameters. Experiments were repeated three times with reproducible results. Scale bar, 10 μm. Right panel: cells were treated with or without ammonium chloride for 1 h and then incubated with 10 μg/ml biotin–transferrin for 30 min. After washing the cell surface, cell lysates were prepared and subjected to immunoblot analysis with anti-biotin antibody. The intensity of each biotin–transferrin band was quantified with a densitometric imager. Cumulative data are presented as a percentage of the cellular biotin-transferrin of control cell protein levels (no inhibitor), and are the means $\pm$ S.E.M. for three independent experiments. *$P < 0.05$. (**D**) Left upper panel: cells were transfected with either control siRNA (siRandom) or siRNA for human transferrin receptor 1 (siTFR1). After 48 h, cells were incubated with Alexa Fluor 488–transferrin for 5 min, and then fluorescence signals were visualized by microscopy as in (**C**). Left lower panel: cells transfected with siRNA were incubated with diferric transferrin (Tf) for 8 h. The cellular iron concentrations before (white bars) or after transferrin (black bars) treatment were measured with a FAAS as in (**A**). Cumulative data are presented as the means $\pm$ S.E.M. for three independent experiments. The iron uptake rate of TFR1-knockdown cells was 31.3 %, compared with control cells ($P < 0.05$). Right panel: cells transfected with siRNA were treated with 5 μM erastin. After incubation for 8 h, the cell death rate was determined by Trypan Blue dye-exclusion assay. Results are the means $\pm$ S.E.M. for three independent experiments.

Free iron released in the endosomes and lysosomes is thought to be involved in local ROS production through the catalysis of Fenton-type reactions [27]. Notably, under basal conditions, intense punctate fluorescent signals produced by PF-TMRos were detected in HT1080 cells (Figures 2A and 4A). These signals overlapped with those produced by LysoSensor dye, a detector of lysosomes, whereas weak membrane-associated signals that were seen behind the spots co-localized with fluorescence produced by MitoTracker Green (Figure 4A). In addition, when HT1080 cells were treated with erastin, increased PF-TMRos signals were partly detected in lysosomes (Figure 4B). These observations suggest that certain reactive oxidants are generated in acidic organelles such as lysosomes as well as in mitochondria. We further analysed the effects of the lysosomal activity inhibitors on basal PF-TMRos signals, and observed that punctate signals were specifically altered in cells with modified lysosome activity (Figure 4C). Baf A_1 or PepA-Me treatment completely eliminated punctate signals, with only a mitochondrial pattern remaining in these cells. In contrast, large punctate signals were concentrated in cells

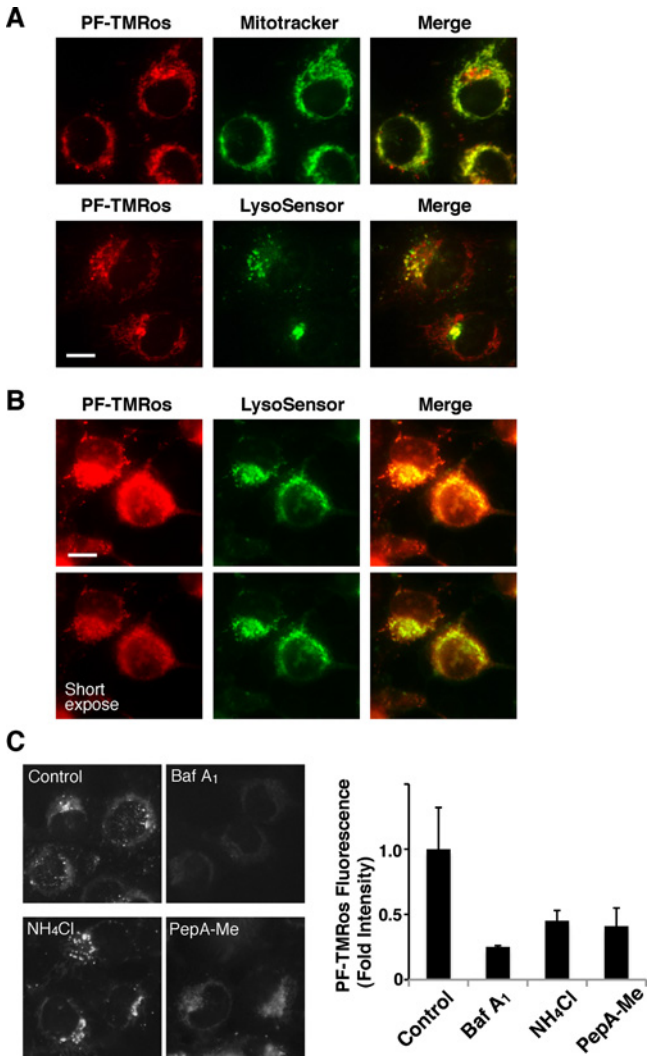

Figure 4 Analysis of intracellular localization of ROS by the redox sensor PF-H_2TMRos

(**A**) HT1080 cells were incubated with 5 μM PF-H_2TMRos and 50 nM MitoTracker (upper panels) or 5 μM PF-H_2TMRos and 5 nM LysoSensor (lower panels). The resulting fluorescence signals were visualized by confocal microscopy with constant fluorescence parameters. Merged images are shown on the right. Experiments were repeated four times with reproducible results. Scale bar, 10 μm. (**B**) Cells treated with 5 μM erastin for 6.5 h were incubated with PF-H_2TMRos and LysoSensor. Fluorescence signals were visualized by microscopy with constant fluorescence parameters (upper panels). PF-TMRos signals with short exposure are shown (lower panels). (**C**) Cells were treated with each inhibitor for 3 h and then incubated with PF-H_2TMRos. Fluorescence signals from PF-TMRos were visualized by microscopy with constant fluorescence parameters. The fluorescence intensity in each cell was quantified with a densitometric imager, and the results from three independent experiments are presented as mean fold-increases $\pm$ S.E.M. compared with that of control cells (untreated). $P < 0.05$.

treated with ammonium chloride. Densitometric measurements revealed that Baf A_1, PepA-Me and ammonium chloride all significantly reduced total cellular fluorescence intensity relative to untreated cells (Figure 4C, histogram). This result suggests that these inhibitors decreased intracellular ROS levels by altering lysosomal activity.

Because massive ROS production in ferroptotic cells was observed mostly in the cytosol (Figures 2A and 4B), lysosomal ROS are probably involved in oxidative cytotoxicity but are not the final determinant. In contrast with the cytosolic ROS burst, lipid-ROS detected in cells undergoing ferroptosis was widely distributed over both organellar and plasma membranes (Figures 5A and 5B, bottom panels). Very low signals from oxidized BODIPY-C_{11} were detected under basal conditions, whereas its distribution shown by red fluorescence was mostly observed in intracellular compartments such as the mitochondria and the endoplasmic reticulum (Figures 5A and 5B, top panels). When cells were treated with erastin or RSL3 for 6 and 2 h, respectively, oxidized signals gradually increased, with their strength varying between individual cells. In erastin-treated cells, membrane peroxidation was detected on both the plasma membrane and the perinuclear compartments shortly after treatment (Figure 5A, middle panels). In contrast, punctate signals appeared around the perinuclear region in RSL3-treated cells before the intensive lipids peroxidation occurred (Figure 5B, middle panels). To investigate the proper localization of oxidized signals, we used marker proteins with a blue fluorescent protein (BFP) tag. The cation-dependent M6PR is localized at the *trans*-Golgi network and subsequent endosomal compartments [28], and the ICT1 is a component of mitochondrial ribosome [29]. The transient transfection analyses revealed that punctate signals observed in early phase of ferroptosis were co-localized with M6PR–BFP2 (Figure 5C, upper panels). This observation suggests that lipid ROS in ferroptotic cells is first generated around Golgi compartments that include endosomes. Meanwhile, increased oxidized signals in late-ferroptotic cells were found in mitochondria, with a ring-like structure surrounding the fragments (Figure 5C, lower panels).

DISCUSSION

Ferroptosis is a novel form of cell death that is dependent on intracellular iron. In primary studies, erastin-induced ferroptosis was predominantly observed in oncogenic Ras-expressed cells [3–5]. This Ras-dependent selectivity could be explained by the finding that these cells accumulate iron by modulating expression levels of ferritin and the transferrin receptor [5]. Iron that is taken up by the transferrin receptor is routed into the endosome/lysosome pathway where ferritin is degraded to release active iron via a specific autophagy pathway. Thus, autophagy and functional lysosomes probably contribute to ferroptosis through the provision of iron, which would seem to be at odds with the earlier finding that 3-MA and Baf A_1 were ineffective at preventing erastin-induced ferroptosis [3]. However, in the present study we demonstrated that treatment with autophagy inhibitors or compounds that alter lysosomal function indeed diminished FIN (e.g. erastin and RSL3)-induced oxidative toxicity in HT1080 and Calu-1 cells (Figure 1 and Supplementary Figure S2). The difference in the results obtained in these two studies may be due to the different time of FIN treatments and inhibitor concentrations. In the present study, we used <1 μg/ml Baf A_1, which was sufficient to prevent the effects of FINs, and also found that treatment with a higher dose induced apoptotic cell death in these cells (results not shown). In contrast, the inhibitory activities of 3-MA and PepA-Me were relatively low, given that they induced cell death in 50 % and 40 % of HT1080 cells, respectively, at the 24 h point (results not shown). However, these reagents could efficiently block ferroptosis following a short-term incubation even in the presence of higher doses of erastin or RSL3 (Figure 1A and results not shown).

We further showed that punctate fluorescence signals produced by the ROS indicator PF-H_2TMRos were present around perinuclear regions in proliferating HT1080 cells, and these signals were specifically reduced in the presence of lysosomal inhibitors (Figure 4C). This result suggests that certain oxidants are localized at acidic compartments such as

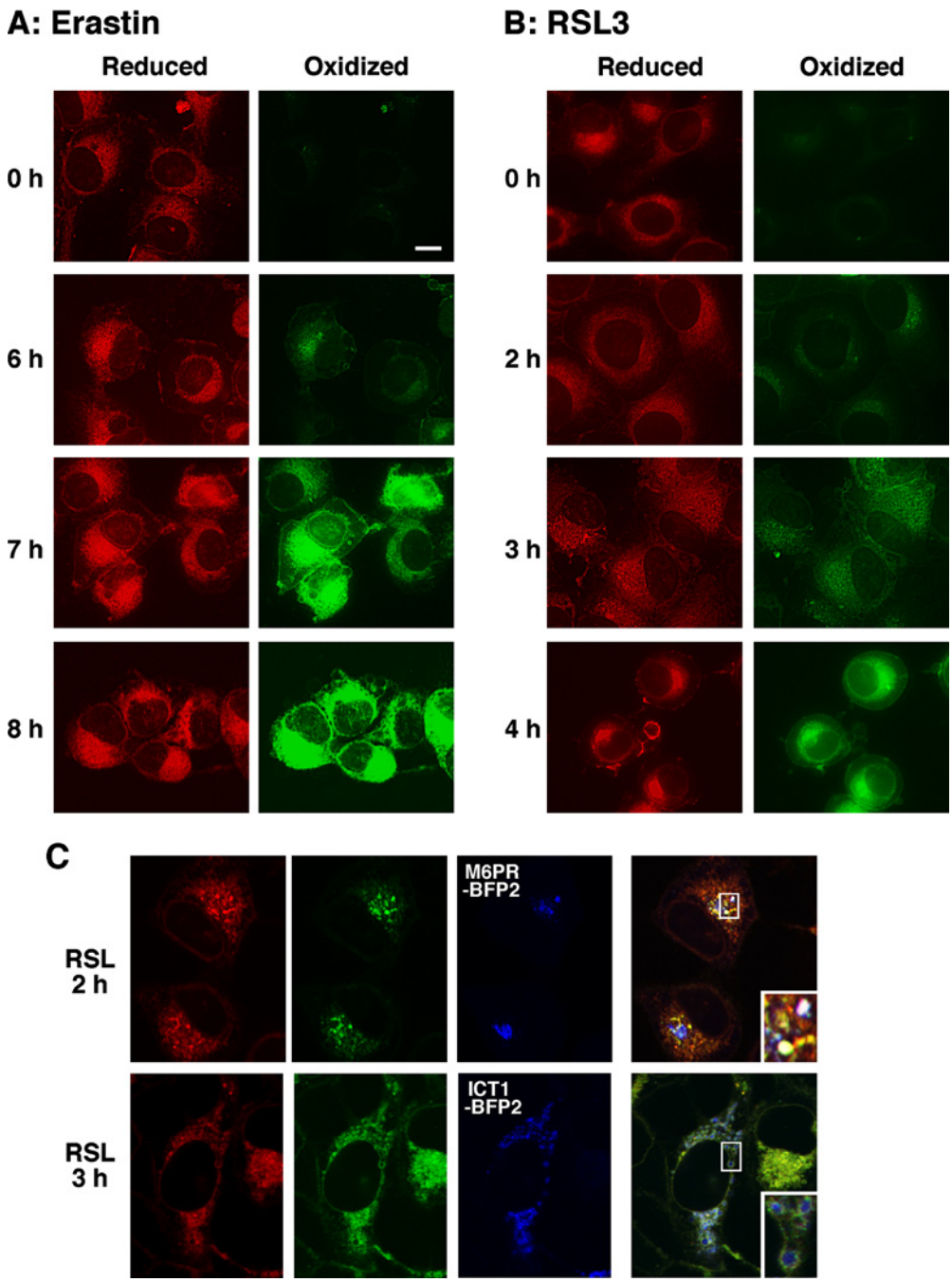

Figure 5 Lipid ROS accumulates in ferroptotic cells

(**A**) HT1080 cells were treated with 5 μM erastin for the indicated time. Cells were incubated with 5 μM BODIPY-(581/591)-C_{11} for 30 min. Green and red fluorescence signals were separately visualized by microscopy with constant fluorescence parameters. (**B**) Cells were treated with 1 μM RSL3 for the indicated time. The cells were treated as in (**A**) and then lipid peroxidation levels were assessed. Scale bar, 10 μm. (**C**) HT1080 cells transfected with M6PR–BFP2 or ICT1–BFP2 were treated with 1 μM RSL3 for the indicated time. Cells were incubated with BODIPY-(581/591)-C_{11}, and fluorescence signals were separately visualized by microscopy with constant fluorescence parameters. Insets show the higher magnification pictures within the boxed areas.

endosomes/lysosomes. Recent studies have shown that selective autophagic degradation of ferritin promotes iron release within lysosomes, and this event, ferritinophagy, is important for cellular iron homoeostasis [24,25]. The observation that treatment of cells with PepA-Me caused both an increase in ferritin protein levels and a decrease in iron content (Figures 3A and 3B) indicated that this inhibitor may diminish ferroptosis by preventing autophagic degradation of ferritin. On the other hand, ammonium chloride promoted a significant reduction in iron uptake by transferrin (Figure 3C). Moreover, TFR1 knockdown attenuated basal ROS (results not shown) and inhibited erastin-induced ferroptosis (Figure 3D). These results indicate that redox-active iron from ferritin or transferrin is presumably involved in local ROS generation within endosomes/lysosomes. Labile iron was shown to be consistently observed in endosomes or lysosomes in primary hepatocytes or hepatocellular carcinoma by iron-specific

fluorescent probes [30,31]. Lysosomal ROS or some ferrous ion [Fe(II)] may relocate to the cytoplasm, which in turn could induce the ROS burst during the FIN-induced oxidative toxicity. In addition, lysosomal ROS and iron may contribute to lipid ROS production because oxidized membranes were observed at the perinuclear compartments during the early phase of ferroptosis (Figure 5). We thus presume that lipid ROS within the endolysosomal membrane triggers iron-mediated chain lipid peroxidation.

Our data suggest that autophagy contributes to ferroptosis through the generation of lysosomal ROS in N-Ras-mutated HT1080 cells. Autophagy appears to have a dual role in cancer progression wherein during the early stages of transformation it suppresses cancer progression, but in later stages it maintains the cancer phenotype [32]. Autophagy is reportedly up-regulated in Ras cancer cells and affects both mitochondrial activity and ROS production [33–36]. ROS generated in lysosomes is included in the total amount of cellular ROS in HT1080 cells (Figure 4C), which is in agreement with previous evidence demonstrating that autophagy elevates cellular ROS levels via the active functions of both mitochondria and lysosomes. Therefore, increased autophagy and ROS production in Ras cancers may provide modest selectivity against ferroptosis. Oncogenic Ras expression has been reported to repress toxic ROS levels by promoting the activity of the NRF2 antioxidant pathway [37], whereas elevated glutathione levels produced by NRF2 pathway activation are also critical for cancer cell proliferation [38,39]. Treatment with lysosomal inhibitors blocks lysosomal ROS production, which may lead to a relative increase in the cellular detoxification activity that is mainly contributed by intracellular GSH.

In the present study, we have shown that pharmacological inhibition of autophagy or lysosomes attenuates drug-induced ferroptosis in tumour cells. Our results suggest that endosomes/lysosomes contribute to this form of cell death by modulating iron equilibria and ROS expression. We further suggest the possibility that lipid ROS are generated at these organelles, which is consistent with a recent observation that in GPx4-deficient cells lipid peroxidation is initiated outside the mitochondria [15]. Further localization analysis with additional specific probes will be required to determine the site of ROS triggers and the critical membrane break involved in ferroptosis.

AUTHOR CONTRIBUTION

Seiji Torii, Ryosuke Shintoku, Chisato Kubota and Keiichi Yamada designed and performed the experiments. Makoto Yaegashi, Ryoko Torii, Toshinobu Suzuki and Masaya Sasaki participated in the experiments. Masanobu Mori, Yuhei Yoshimoto and Toshiyuki Takeuchi supervised the present study and critically read the paper. Seiji Torii analysed the data and wrote the paper.

ACKNOWLEDGEMENTS

We thank Dr M. Naito (National Institute of Health Sciences), Dr N. Nameki, Dr T. Oda (Gunma University), Dr Y. Kato, Dr K. Nakayama and Dr Y. Takeda (Kyoto University) for technical advice and helpful discussion. We also thank Ms E. Tajima and Ms M. Hosoi for their generous support.

FUNDING

This work was supported by the Japanese Society for the Promotion of Science (JSPS KAKENHI) [grant number 24390050]; and the Institute for Molecular and Cellular Regulation, Gunma University [grant number 14036].

REFERENCES

1 Vanden Berghe, T., Linkermann, A., Jouan-Lanhouet, S., Walczak, H. and Vandenabeele, P. (2014) Regulated necrosis: the expanding network of non-apoptotic cell death pathways. Nat. Rev. Mol. Cell Biol. **15**, 135–147 CrossRef PubMed
2 Reed, J.C. and Pellecchia, M. (2012) Ironing out cell death mechanisms. Cell **149**, 963–965 CrossRef PubMed
3 Dixon, S.J., Lemberg, K.M., Lamprecht, M.R., Skouta, R., Zaitsev, E.M., Gleason, C.E., Patel, D.N., Bauer, A.J., Cantley, A.M., Yang, W.S. et al. (2012) Ferroptosis: an iron-dependent form of nonapoptotic cell death. Cell **149**, 1060–1072 CrossRef PubMed
4 Yagoda, N., von Rechenberg, M., Zaganjor, E., Bauer, A.J., Yang, W.S., Fridman, D.J., Wolpaw, A.J., Smukste, I., Peltier, J.M., Boniface, J.J. et al. (2007) RAS-RAF-MEK-dependent oxidative cell death involving voltage-dependent anion channels. Nature **447**, 864–868 CrossRef PubMed
5 Yang, W.S. and Stockwell, B.R. (2008) Synthetic lethal screening identifies compounds activating iron-dependent, nonapoptotic cell death in oncogenic-RAS-harboring cancer cells. Chem. Biol. **15**, 234–245 CrossRef PubMed
6 Yang, W.S., SriRamaratnam, R., Welsch, M.E., Shimada, K., Skouta, R., Viswanathan, V.S., Cheah, J.H., Clemons, P.A., Shamji, A.F., Clish, C.B. et al. (2014) Regulation of ferroptotic cancer cell death by GPX4. Cell **156**, 317–331 CrossRef PubMed
7 Skouta, R., Dixon, S.J., Wang, J., Dunn, D.E., Orman, M., Shimada, K., Rosenberg, P.A., Lo, D.C., Weinberg, J.M., Linkermann, A. and Stockwell, B.R. (2014) Ferrostatins inhibit oxidative lipid damage and cell death in diverse disease models. J. Am. Chem. Soc. **136**, 4551–4556 CrossRef PubMed
8 Thomas, J.P., Geiger, P.G., Maiorino, M., Ursini, F. and Girotti, A.W. (1990) Enzymatic reduction of phospholipid and cholesterol hydroperoxides in artificial bilayers and lipoproteins. Biochim. Biophys. Acta **1045**, 252–260 CrossRef PubMed
9 Imai, H., Hirao, F., Sakamoto, T., Sekine, K., Mizukura, Y., Saito, M., Kitamoto, T., Hayasaka, M., Hanaoka, K. and Nakagawa, Y. (2003) Early embryonic lethality caused by targeted disruption of the mouse PHGPx gene. Biochem. Biophys. Res. Commun. **305**, 278–286 CrossRef PubMed
10 Yant, L.J., Ran, Q., Rao, L., Van Remmen, H., Shibatani, T., Belter, J.G., Motta, L., Richardson, A. and Prolla, T.A. (2003) The selenoprotein GPX4 is essential for mouse development and protects from radiation and oxidative damage insults. Free Radic Biol. Med. **34**, 496–502 CrossRef PubMed
11 Winkler, A., Njalsson, R., Carlsson, K., Elgadi, A., Rozell, B., Abraham, L., Ercal, N., Shi, Z.Z., Lieberman, M.W., Larsson, A. and Norgren, S. (2011) Glutathione is essential for early embryogenesis–analysis of a glutathione synthetase knockout mouse. Biochem. Biophys. Res. Commun. **412**, 121–126 CrossRef PubMed
12 Seiler, A., Schneider, M., Forster, H., Roth, S., Wirth, E.K., Culmsee, C., Plesnila, N., Kremmer, E., Radmark, O., Wurst, W. et al. (2008) Glutathione peroxidase 4 senses and translates oxidative stress into 12/15-lipoxygenase dependent- and AIF-mediated cell death. Cell. Metab. **8**, 237–248 CrossRef PubMed
13 Li, Y., Maher, P. and Schubert, D. (1997) A role for 12-lipoxygenase in nerve cell death caused by glutathione depletion. Neuron **19**, 453–463 CrossRef PubMed
14 Linkermann, A., Skouta, R., Himmerkus, N., Mulay, S.R., Dewitz, C., De Zen, F., Prokai, A., Zuchtriegel, G., Krombach, F., Welz, P.S. et al. (2014) Synchronized renal tubular cell death involves ferroptosis. Proc. Natl. Acad. Sci. U.S.A. **111**, 16836–16841 CrossRef PubMed
15 Friedmann Angeli, J.P., Schneider, M., Proneth, B., Tyurina, Y.Y., Tyurin, V.A., Hammond, V.J., Herbach, N., Aichler, M., Walch, A., Eggenhofer, E. et al. (2014) Inactivation of the ferroptosis regulator Gpx4 triggers acute renal failure in mice. Nat. Cell. Biol. **16**, 1180–1191 CrossRef PubMed
16 Hentze, M.W., Muckenthaler, M.U., Galy, B. and Camaschella, C. (2010) Two to tango: regulation of mammalian iron metabolism. Cell **142**, 24–38 CrossRef PubMed
17 Irani, K., Xia, Y., Zweier, J.L., Sollott, S.J., Der, C.J., Fearon, E.R., Sundaresan, M., Finkel, T. and Goldschmidt-Clermont, P.J. (1997) Mitogenic signaling mediated by oxidants in Ras-transformed fibroblasts. Science **275**, 1649–1652 CrossRef PubMed
18 Mitsushita, J., Lambeth, J.D. and Kamata, T. (2004) The superoxide-generating oxidase Nox1 is functionally required for Ras oncogene transformation. Cancer Res. **64**, 3580–3585 CrossRef PubMed
19 Minotti, G. and Aust, S.D. (1987) The requirement for iron (III) in the initiation of lipid peroxidation by iron (II) and hydrogen peroxide. J. Biol. Chem. **262**, 1098–1104 PubMed
20 Stockwell, B.R., Yang, W.S. and SriRamaratnam, R. (2010) Oncogenic-RAS-signal dependent lethal compounds. U.S. Pat. 8,546,421 B1
21 Kubota, C., Torii, S., Hou, N., Saito, N., Yoshimoto, Y., Imai, H. and Takeuchi, T. (2010) Constitutive reactive oxygen species generation from autophagosome/lysosome in neuronal oxidative toxicity. J. Biol. Chem. **285**, 667–674 CrossRef PubMed
22 Hou, N., Mogami, H., Kubota-Murata, C., Sun, M., Takeuchi, T. and Torii, S. (2012) Preferential release of newly synthesized insulin assessed by a multi-label reporter system using pancreatic beta-cell line MIN6. PLoS One **7**, e47921 CrossRef PubMed

23 Fujita, N., Hayashi-Nishino, M., Fukumoto, H., Omori, H., Yamamoto, A., Noda, T. and Yoshimori, T. (2008) An Atg4B mutant hampers the lipidation of LC3 paralogues and causes defects in autophagosome closure. Mol. Biol. Cell **19**, 4651–4659 CrossRef PubMed

24 Asano, T., Komatsu, M., Yamaguchi-Iwai, Y., Ishikawa, F., Mizushima, N. and Iwai, K. (2011) Distinct mechanisms of ferritin delivery to lysosomes in iron-depleted and iron-replete cells. Mol. Cell. Biol. **31**, 2040–2052 CrossRef PubMed

25 Mancias, J.D., Wang, X., Gygi, S.P., Harper, J.W. and Kimmelman, A.C. (2014) Quantitative proteomics identifies NCOA4 as the cargo receptor mediating ferritinophagy. Nature **509**, 105–109 CrossRef PubMed

26 Chan, R.Y., Ponca, P. and Schulman, H.M. (1992) Transferrin-receptor-independent but iron-dependent proliferation of variant Chinese hamster ovary cells. Exp. Cell Res. **202**, 326–336 CrossRef PubMed

27 Terman, A. and Kurz, T. (2013) Lysosomal iron, iron chelation, and cell death. Antioxid. Redox Signal. **18**, 888–898 CrossRef PubMed

28 Puertollano, R., Aguilar, R.C., Gorshkova, I., Crouch, R.J. and Bonifacino, J.S. (2001) Sorting of mannose 6-phosphate receptors mediated by the GGAs. Science **292**, 1712–1716 CrossRef PubMed

29 Pagliarini, D.J., Calvo, S.E., Chang, B., Sheth, S.A., Vafai, S.B., Ong, S.E., Walford, G.A., Sugiana, C., Boneh, A., Chen, W.K. et al. (2008) A mitochondrial protein compendium elucidates complex I disease biology. Cell **134**, 112–123 CrossRef PubMed

30 Ma, Y., de Groot, H., Liu, Z., Hider, R.C. and Petrat, F. (2006) Chelation and determination of labile iron in primary hepatocytes by pyridinone fluorescent probes. Biochem. J. **395**, 49–55 CrossRef PubMed

31 Au-Yeung, H.Y., Chan, J., Chantarojsiri, T. and Chang, C.J. (2013) Molecular imaging of labile iron(II) pools in living cells with a turn-on fluorescent probe. J. Am. Chem. Soc. **135**, 15165–15173 CrossRef PubMed

32 Bellot, G.L., Liu, D. and Pervaiz, S. (2013) ROS, autophagy, mitochondria and cancer: Ras, the hidden master? Mitochondrion **13**, 155–162 CrossRef PubMed

33 Weinberg, F., Hamanaka, R., Wheaton, W.W., Weinberg, S., Joseph, J., Lopez, M., Kalyanaraman, B., Mutlu, G.M., Budinger, G.R. and Chandel, N.S. (2010) Mitochondrial metabolism and ROS generation are essential for Kras-mediated tumorigenicity. Proc. Natl. Acad. Sci. U.S.A. **107**, 8788–8793 CrossRef PubMed

34 Lock, R., Roy, S., Kenific, C.M., Su, J.S., Salas, E., Ronen, S.M. and Debnath, J. (2011) Autophagy facilitates glycolysis during Ras-mediated oncogenic transformation. Mol. Biol. Cell **22**, 165–178 CrossRef PubMed

35 Guo, J.Y., Chen, H.Y., Mathew, R., Fan, J., Strohecker, A.M., Karsli-Uzunbas, G., Kamphorst, J.J., Chen, G., Lemons, J.M., Karantza, V. et al. (2011) Activated Ras requires autophagy to maintain oxidative metabolism and tumorigenesis. Genes Dev. **25**, 460–470 CrossRef PubMed

36 Kim, M.J., Woo, S.J., Yoon, C.H., Lee, J.S., An, S., Choi, Y.H., Hwang, S.G., Yoon, G. and Lee, S.J. (2011) Involvement of autophagy in oncogenic K-Ras-induced malignant cell transformation. J. Biol. Chem. **286**, 12924–12932 CrossRef PubMed

37 DeNicola, G.M., Karreth, F.A., Humpton, T.J., Gopinathan, A., Wei, C., Frese, K., Mangal, D., Yu, K.H., Yeo, C.J., Calhoun, E.S. et al. (2011) Oncogene-induced Nrf2 transcription promotes ROS detoxification and tumorigenesis. Nature **475**, 106–109 CrossRef PubMed

38 Recktenwald, C.V., Kellner, R., Lichtenfels, R. and Seliger, B. (2008) Altered detoxification status and increased resistance to oxidative stress by K-ras transformation. Cancer Res. **68**, 10086–10093 CrossRef PubMed

39 Mitsuishi, Y., Taguchi, K., Kawatani, Y., Shibata, T., Nukiwa, T., Aburatani, H., Yamamoto, M. and Motohashi, H. (2012) Nrf2 redirects glucose and glutamine into anabolic pathways in metabolic reprogramming. Cancer Cell **22**, 66–79 CrossRef PubMed

Received 5 June 2015/21 December 2015; accepted 12 January 2016
Accepted Manuscript online 12 January 2016, doi:10.1042/BJ20150658